

Journal of Materials Chemistry C

Accepted Manuscript



This is an *Accepted Manuscript*, which has been through the Royal Society of Chemistry peer review process and has been accepted for publication.

Accepted Manuscripts are published online shortly after acceptance, before technical editing, formatting and proof reading. Using this free service, authors can make their results available to the community, in citable form, before we publish the edited article. We will replace this *Accepted Manuscript* with the edited and formatted *Advance Article* as soon as it is available.

You can find more information about *Accepted Manuscripts* in the [Information for Authors](#).

Please note that technical editing may introduce minor changes to the text and/or graphics, which may alter content. The journal's standard [Terms & Conditions](#) and the [Ethical guidelines](#) still apply. In no event shall the Royal Society of Chemistry be held responsible for any errors or omissions in this *Accepted Manuscript* or any consequences arising from the use of any information it contains.

Well-designed Metal Nanostructured Array for Label-free Plasmonic Biosensing

Wanbo Li^a, Li Zhang^a, Jianhua Zhou^{a*}, and Hongkai Wu^{b*}

5

a Prof. J. H. Zhou, W. B. Li, L. Zhang

Key Laboratory of Sensing Technology and Biomedical Instruments of Guangdong Province,
School of Engineering, Sun Yat-sen University,

10 Guangzhou 510006, China

b Prof. H. K. Wu

Department of Chemistry

15 The Hong Kong University of Science and Technology

Clear Water Bay, Kowloon, Hong Kong, China

20 *Corresponding author. Tel.: +86 20 39387890; Fax: +86 20 39387890.

E-mail: zhoujh33@mail.sysu.edu.cn (J. H. Zhou); chhkwwu@ust.hk (H. K. Wu)

Abstract:

Localized surface plasmon resonance (LSPR) can concentrate light into nanometer-scale spatial regions, which arouse the sensitivity to local refractive index change in response to the analytes at or near the metal surfaces. LSPR-based nanostructured materials have great potential to be developed into large-scale arrays composed of highly miniaturized and uniform signal transducer elements, thereby initiating high throughput screening platform for refractometric biosensing. In this review, we present an overview of these nanostructured materials with LSPRs and their applications in biosensing. Firstly, we give an introduction of the study of both fundamental and practical aspects of localized surface plasmon excitations in metal materials, and then the review focuses on some well-designed nanostructures in particular thin perforated film and some quasi-three-dimensional structures, each nanostructure is detailed and the plasmonic properties of them are briefly described. After that, a brief summary of the fabrication methods for plasmonic nanostructures are presented. Finally, the future research trends of plasmonic biosensing are highlighted and a conclusion with perspectives is given.

15

Keywords: localized surface plasmon resonance; nanostructured materials; biosensor

1. Introduction

The mirror-like quality of smooth noble-metal films changes markedly when the metal is separated into particles that are smaller than the wavelength of light, which enables great applications in biosensing, as well as many other important energy areas. This great change is due to a physical phenomenon, known as localized surface plasmon resonance (LSPR) induced by metal nanoparticles or nanostructures concentrates light into a nano-size region, leading to enormous applications, such as enhancement of nonlinear effect¹, surface enhanced Raman scattering (SERS)² and refractive index sensing³. The mechanism of LSPR biosensing using these metal nanostructures is that, the intense surface plasmon absorption bands and the enhancement of the local electromagnetic fields, owing to the excitation of charge density oscillations by light, are highly sensitive to the local refractive index change in response to the analytes at or near the surfaces of the metal nanostructures. Compared to the commercial surface plasmon resonance refractive index sensor, LSPR refractive index sensor is simple, cost effective and suitable to measure the short-range changes in the local refractive index induced by the adsorbed molecules⁴.

LSPR generation is theoretically possible in any metal, alloy or semiconductor with a large negative real dielectric constant and small imaginary part of the dielectric constant, while the vast majority of LSPR sensing experiments have been carried out on gold or silver. Gold is preferred biological application in many literatures, because of its chemical inert nature, resistance to oxidation, and biocompatibility⁵, and thiol-gold association that have been well developed for immobilization of biomolecules⁶. Though being easily oxidisable under ordinary laboratory conditions, silver is popular material for LSPR at visible frequencies due to the narrow plasmon line width, which is ascribed to its intrinsic optical properties. Recent years have seen considerable development in the aluminum LSPR biosensing which take advantages of its LSPR exhibits in the ultraviolet (UV) to blue wave region⁷, and many other attractive properties, including low cost, high natural abundance, and ease of processing by a wide variety of methods including complementary metal oxide semiconductor (CMOS). In addition to the above-mentioned materials, some other metals (e.g. copper⁸, palladium⁹) and semiconductors as graphene¹⁰ are also candidates as plasmonic materials, however are rarely used for biosensing.

Driven by the increasing need for sensitive, fast, cost-effective, low-reagent-consumption and ease-of-use biosensors for applications in the clinical and biomedical field, a myriad of

well-designed plasmonic nanostructures^{8, 11-15} has appeared in the literature during the last decades. From the currently sophisticated fabrication technologies, optical biosensing based on metal nanostructure arrays show unquestionable advantages compared with single particle sensing. (1) The shape, size, composition and spacing of the nanoparticles can be readily controlled to provide tunable plasmonic peak position and width. (2) Metallic nanostructures linked to surfaces are free of capping agents, and better stable in aggressive environments (*e.g.* changes in the ionic strength, pH or temperature), making the surface readily accessible for functionalization with specific receptors or ligands, and being easily cleaned and reused if needed. (3) Nanostructure based biosensors hold great potential for multiplexing and miniaturization on highly integrated device. (4) Above all, the biosensing schemes based on arrays of nanostructures not only offer improved possibilities for cheap and mass-scale chip production, but also hold the advantage of keeping the required instrumentation very simple. It comes therefore as no surprise that most nanoplasmonic biosensing studies currently rely on the use of nanostructured substrates, which hence, are considered to be key components for the creation of advanced biosensing platforms. This review therefore focuses on some well-designed plasmonic nanostructured and their applications in biosensing. The similar plasmonic structures while made from different materials will be presented if available in the literatures. After that, there will be a brief overview of the micro-/nano- fabrication methods employed to plasmonic nanostructure generation; both advantages and disadvantages, as well as the application areas will be listed. Finally, the future research trends of plasmonic biosensing are highlighted and a conclusion with perspectives is given.

2. Metal nanostructured arrays for biosensing

Plasmonics from well-designed nanostructures has been an active area of research due, in part, to their growing importance in biosensing and imaging; whilst thanks to the recent advances in nanofabrication methodologies^{16, 17}, the formation of well-designed metal nanostructures with advanced plasmonic properties could be pre-designed and obtained. These methodologies have led to the realization of two dimensional (2D) or Quasi-three-dimensional (Q3D) metal nanostructures composed of nanoparticles¹⁸, nanoholes¹⁹, nanopillars¹⁵, and other components²⁰, providing excellent properties as listed above when applied to biosensing.

2.1. 2D nanostructure array

2.1.1. Nanohole array film

One of the central nanostructured substrate employed for biosensing is nanohole array, which takes advantage of an optical phenomenon referred to as extraordinary optical transmission (EOT) at periodic nanostructures in films made from perfect conductors. In 1998, Ebbesen and co-workers²¹ reported an extraordinary light transmission through square arranged holes (150 nm diameter) fabricated by a focused ion beam through 200 nm thick silver films. The transmission of light through otherwise opaque metallic films occurs at plasmon resonant wavelengths upon the confinement of surface plasmons to the near-interface region between the metal and the dielectric, causing the material seemed much more transparent than it should be. Those following years have seen lots of investigation focused on EOT²¹, revealing that, the peaks of maximum transmission were related to the distance between the nanoholes (periodicity) and the EOT effect was observed for different metal materials as well, such as gold and aluminum films, but its magnitude decreased when different metals were used. So far, the interpretation has since been challenged yet, the evidence from several laboratories seems to consolidate the excitation of surface plasmon as the main contribution to the EOT effect²².

As sensing elements, nanohole arrays present unique advantages, including a high reproducibility level, multiplexing capabilities and the possibility for collinear optical integration. The nanohole array is obtained facily by various methods²³. Moreover, it could be used in transmission mode, especially the normal transmission LSPR (T-LSPR) ones²⁴ (see the details in section 4), enabling easy-of-use refractometric biosensing with simple and low-cost measurement configuration, which is more attractive in comparison. Experiencing the development along through single substrate, single channel to multiple substrate with complex fluidic structures for multiple and parallel analysis, the operation of the nanohole array LSPR sensing, availing itself of the porous property, have now established two modalities, that is the so-called flow-over and flow-through sensing (Fig. 1). A. Lesuffleur and his co-authors¹¹ reported a microfluidic device with integrated gold-nanohole-array-based chemical and biological sensors, which took advantages of the unique properties of nanohole arrays: surface-based sensitivity, transmission mode operation, a relatively small footprint, and good repeatability. This platform, shown schematically in Fig. 1A, was formed of periodically (350 to 850 nm) arranged arrays of 150 nm diameter nanoholes fabricated via focus

ion beam (FIB) milling, with square footprints in the order of $400 \mu\text{m}^2$. The real-time transmission signals in response to solutions with different concentrations of analytes were monitored when they flowed over the surface of the porous film (Fig. 1B), with the refractive index sensitivity determined to be 333 nm/RIU. The device was also capable of detecting spatial microfluidic concentration gradients and to monitor a biochemical affinity process involving the biotin–streptavidin system. This first set of experiments demonstrated the potential of on-chip nanohole array based sensing platforms, adding unique surface-sensitive diagnostic capabilities to the existing suite of microfluidic-based analytical tools. Fig 1C shows the other sensing modality, *i.e.* flow-through sensing²⁵, in which, the analyte solution flow through the nanoholes in the free-standing film. The integrated chip was interfaced with external pressure-control hardware to facilitate the delivery of fluid passing through the arrays from the nitride. This method was firstly demonstrated by F. Eftekhari and his co-authors. Compared with the flow-over one that commonly conducted on the dead-ended holes array, the presented one resulted in a 6-fold improvement in response time (Fig. 1D). The flow-through nanohole sensing platform was then applied to label-free monitor the formation of a monolayer and the immobilization of an ovarian cancer biomarker specific antibody on the sensing surface in real-time at a concentration of 80 nM.

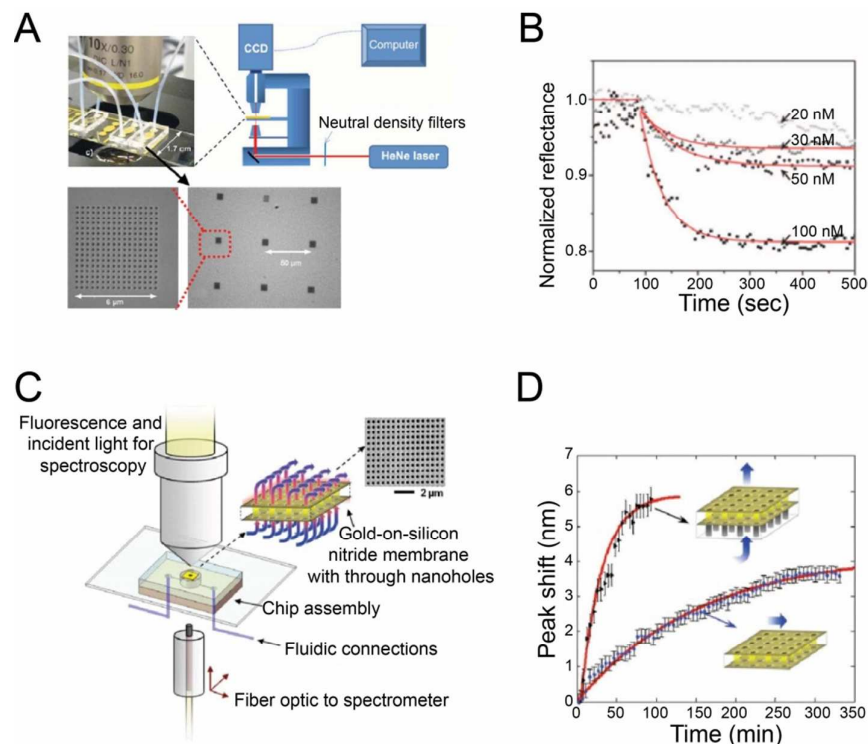


Figure 1. Nanohole array sensing using two perform modalities. (A) Schematic of the experimental setup for flow-over sensing; picture of the integrated on-chip nanohole array platform, and SEM images of the nanohole array arrangement contained within the platform. (B) Real-time monitoring of streptavidin–biotin binding for different concentrations of streptavidin. Reproduced with permission from Reference 11. Copyright 2008 Optical Society of America. (C) Schematic of the optical and fluidic test setup employed for both fluorescence tests and transmission spectroscopy. (D) Comparison of response to surface adsorption achieved with flow-over and flow-through formats as indicated in the insets. Measured peak shift (at 625 nm) is plotted as a function of time during flow through/over of an ethanol/11-mercaptoundecanoic acid (MUA) solution. As indicated in the inset, the flow-through sensor is operated with flow from the non-participating silicon nitride side to the active gold surface. Reproduced with permission from Reference 25. Copyright 2009 American Chemical Society.

Apart from the silver and gold nanohole array, J. L. Skinner et al.²⁶ explored the possibility of biosensing using aluminum nanohole array which was made a comparison with silver nanohole array. Both of arrays, with periodicity of 500 nm and nanohole diameter of 110 nm, were fabricated through nanoimprint lithography (NIL). The optical investigation showed that the plasmon resonance

wavelengths and the refractive index sensitivities of Ag and Al nanohole arrays were almost the same (~510 nm/RIU) (Fig. 2A), respectively, and were comparable with the gold ones. After that, the aluminum nanohole sensing was brought into more complicated sensing system which involved specific recognition. Víctor Canalejas-Tejero and his co-authors²⁷ prepared an aluminum nanohole array by electron beam lithography (EBL). The substrate was demonstrated to be good device resistance against pitting and oxidation, and was applied to immuno-detection of biotin at a concentration of 2 $\mu\text{g/mL}$ (Fig. 2B). C. A. Barrios et al.²⁸ fabricated an aluminum nanohole array optical biosensor on polycarbonate substrate and applied it to cost-effective, portable optical biosensing of biotin (200 ng/mL) using a competitive inhibition immunoassays strategy (Fig. 2C). This aluminum nanohole biosensor held good performance and low cost which made the presented LSPR-based device a promising candidate for mass-produced label-free optical biosensors on chips.

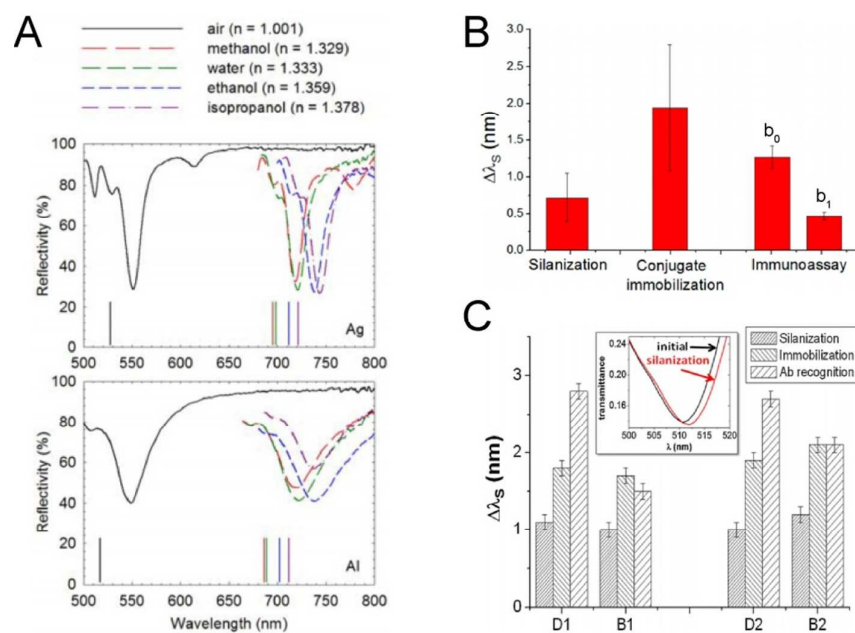


Figure 2. Aluminum nanohole array for biosensing. (A) Reflectivity data for (top) Ag grating and (bottom) Al grating covered with different fluids. The spectral location of reflectivity minima increases with refractive index. Reproduced with permission from Reference 26. Copyright 2008 IEEE. (B) Red-shifts of reflectivity minima measured after silanization, conjugate immobilization, direct assay (b₀), and competitive assay (b₁) experiments. Reproduced with permission from Reference 27. Copyright 2014 American Chemical Society. (C) S-wavelength variation for direct and competitive assays carried out on the fabricated Al nanohole arrays on polycarbonate substrates. Dense, medium and sparse patterns correspond to wavelength shifts after sensor surface silanization, functionalization on silanized surfaces and antibody

(Ab) incubation, respectively. D1=direct assay with [Ab]=1 $\mu\text{g}/\text{mL}$ and 20-min incubation; B1=competitive assay with [Ab]=1 $\mu\text{g}/\text{mL}$ and 20-min incubation; D2=direct assay with [Ab]=0.2 $\mu\text{g}/\text{mL}$ and 60-min incubation; B2=competitive assay with [Ab]=0.2 $\mu\text{g}/\text{mL}$ and 60-min incubation. The inset shows the measured spectral transmittances around the S-resonance before (black line) and after (red line) silanization (assay B2). Reproduced with permission from Reference 28. Copyright Springer Science+Business Media New York 2014.

2.1.2. Metal island

Metal nanoparticles based subwavelength antennas, placed in direct contact with the glass or polymer substrate, are also promising candidate for refractometric biosensing. A simple and facile approach for generation metal island is to direct evaporate a thin metal film with several nanometer thickness²⁹. More efforts, by physical and chemical strategies^{30, 31}, have been made to deposit uniform shaped nanoparticles onto the substrate. However, metal islands created through these methods suffer from inherent drawbacks as uncontrollable orientation and inter space among the nanoparticles, resulting in high full width at the half maximum (FWHM) value and low reproducibility among substrates; these impacts are even huge on the smaller-area metal island, which goes against mass-integration biosensing. A worth-mentioning device prepared by deposition method is the gold nanoprism monolayer film. Y. H. Lee and his co-workers¹² employed Langmuir-Schaefer technique created large-area close-packed monolayer gold nanotriangles at the air-water interface. It came no surprise that the peak width was too wide for peak-shift based sensing. The authors thereafter applied these substrates to SERS.

Van duyne's group invented a well-designed method relied on closely packed nanosphere for ordered 2D nanoparticle array with controlled shape, size, and interparticle spacing generation, so-called nanosphere lithography (NSL)^{31, 32}, which is inexpensive, simple to implement, inherently parallel, high throughput. The NSL is begun with the self-assembly of size-monodisperse nanospheres with a desire diameter to form a two-dimensional colloidal crystal deposition mask; Following self-assembly of the nanosphere mask, a metal or other material is then deposited by thermal evaporation or other methods. After metal deposition, the nanosphere mask is removed by sonicating the entire sample in a solvent, leaving behind the material deposited through the nanosphere mask to the substrate. Besides, a new class of NSL structures has been developed by

varying the angle between the nanosphere mask and the beam of material being deposited (Fig 3A). This technique is hereafter referred to as angle-resolved NSL (AR NSL)³³. Interesting applications of AR NSL³² include generations of nanooverlap structures (Fig 3B), nanogap structures (Fig 3C), and nanoparticle chains (Fig 3C) by sequential steps of first normal deposition and then oblique deposition of material through a nanosphere mask.

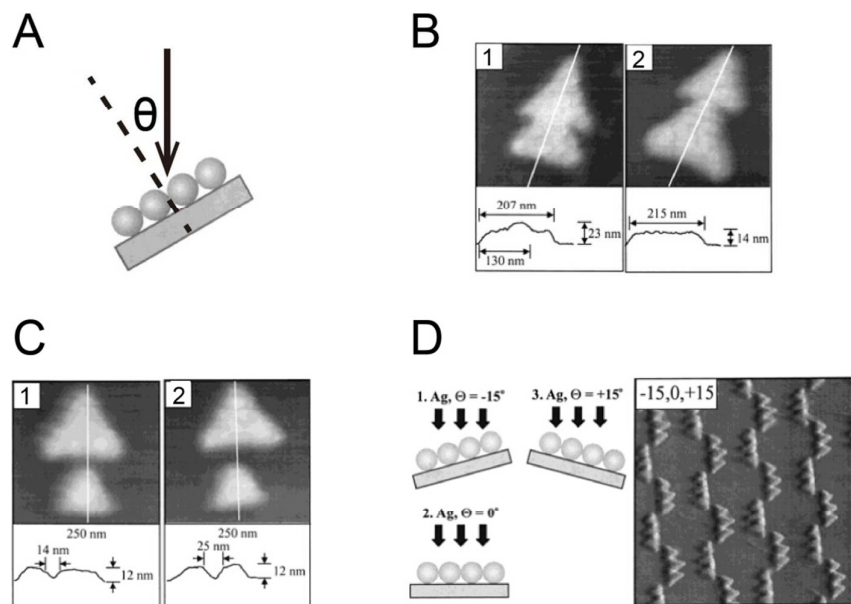
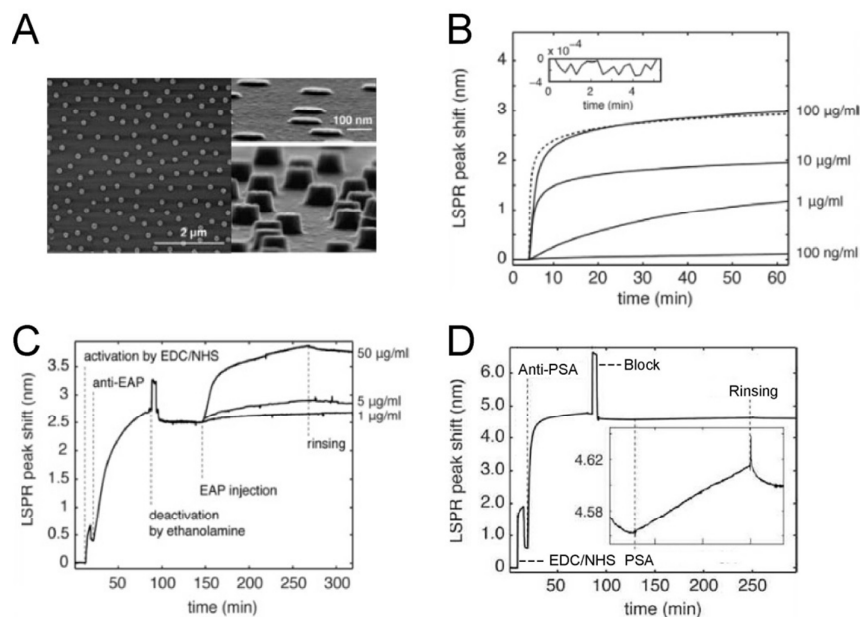


Figure 3. (A) Geometry shows the AR NSL. (B) Nanooverlap structures, (C) nanogap structures, and (D) nanoparticle chains generated through AR NSL. The nanoparticle chains generation was schematically illustrated in the left of (D). Reproduced with permission from Reference 32. Copyright 2001 American Chemical Society.

Colloid lithography is also a useful method for generating metal column on substrate. S. Chen et al.¹³ have shown an LSPR sensor (Fig. 4A) with a greatly decreased noise level of 0.0001 nm in the LSPR peak wavelength. Though arranged out-of-order, the strong extinction of these nanoparticles array makes extremely accurate peak fitting possible, greatly reducing noise level on measurements of the LSPR peak. Probed by the adsorption of biotinylated bovine serum albumin (bBSA) on the surface of the sensor, the limit of detection (LOD) for biomolecular sensing was estimated to be 4 bBSA molecules per 100 nanodisks (Fig. 4B). Reliable detection of extracellular adherence protein (EAP) is also readily achieved using this platform, with the LOD estimated to be 8 pM (Fig. 4C). The propose method carried out real-time sensing of prostate-specific antigen (PSA) on anti-PSA

functionalization, with a limit of detection 30 pM, which was estimated to be equivalent to about 15 molecules per nanoparticle (Fig. 4D). In a typical blood sample, the amount of bacteria is less than 30 per milliliter, which indicates that high femtomolar sensitivity would assure a reliable working too for *S. aureus* diagnosis.



5

Figure 4. (A) Top- and side-view scanning electron microscope (SEM) images of the nanodisk array prepared by colloid lithography. (B) bBSA adsorption kinetics monitored as the LSPR shift with time. The inset plots first 5 min of the kinetics. (C) Complete kinetics series, starting with functionalization of the nanodisk array, followed by the EDC/NHS activation, binding of anti-EAP, surface deactivation and finally the detection of EAP solution at three different concentrations, (D) The adsorption series for binding PSA starts with the activation, functionalization, block, and PSA sensing. The inset is a zoom of the kinetics curve region directly adjacent to the inset box. Reproduced with permission from Reference 13. Copyright 2009 IOP Publishing Ltd.

15 Successful operation of the LSPR nanobiosensor in a solution environment was demonstrated by measuring the optical sensitivity to the changes in local refractive index that occur at the metal/liquid interface^{34, 35}. Normally, the LSPR λ_{max} shift was monitored as the changes in the refractive index of the bulk liquids, produced by exposing the Ag nanoparticles (as nanoislands) to methanol, acetone, ethanol, methylene chloride, and benzene; the sensitivities of bare array and self-assembly monolayer modified Ag array were determined to be 190 and 150 nm/RIU, which are far below the

20

ones of Q3D nanostructures reviewed in the next part. The nanoparticles array was applied to a proof-of-concept biological binding event sensing, in which, the LSPR λ_{\max} shift of single layer of periodic Ag nanoparticles array dosed with a mixed monolayer of MUA and 1-octanethiol was monitored to detect the binding of the multiply charged polypeptide, poly-(L)-lysine. In brief, though the NSLs and colloid lithography are capable of direct generation of nanoparticle array on substrate, the refractive index sensitivity should be further improved to meet the needs of label-free biosensing of trace bio-analytes.

2.1.3. Nanoparticle cluster arrays

10 B. M. Reinhard's group³⁶⁻³⁸ invented an advanced nanostructure array called nanoparticle cluster arrays (NCAs) through template-guided chemical self-assembly method. Briefly, a regular structure of wells is created in a poly(methyl methacrylate) (PMMA) film on top of gold film using e-beam lithography, and then gold nanoparticles are electrostatic-assisted self-assembled on the gold surface at the bottom of each well (Fig. 5A). By combining top-down and bottom-up fabrication
15 strategies, it seems that they could overcome some of the limitations of different fabrication methods summarized in section 3. The approach allows reproducible fabrication of arrays with interparticle separations of less than 10 nm, and provides precise control of the structural parameters: the average number of nanoparticles in the clusters (n), the edge-to-edge separation (A), and the diameter of the nanoparticles (d), as showed in Fig. 5B-D. NCAs sustain near-field coupling between particles on
20 multiple length scales (intracluster and inter-cluster separation), which generates a multiscale cascade field enhancement, in which, the multiscale E-field enhancement between the clusters provides a strategy for boosting the E-field enhancement beyond the limit of the individual clusters. L. L. Yang and his co-authors³⁷ demonstrated that optimized ($D = 200$ nm, $A = 50$ nm, $d = 80$ nm) NCAs show the overall highest signal reproducibility and achieve effective single cell detection sensitivity. The
25 SERS spectra of *B.cereus* was recorded with an active laser spot size of 1.5 μm diameter which is similar in size to a typical single bacterial cell (Fig. 5E). The NCA also enables detection of ultra-trace nitroaromatic gas, with the entire monitored concentration range determined to be 10-100 ppb³⁸ (Fig. 5F).

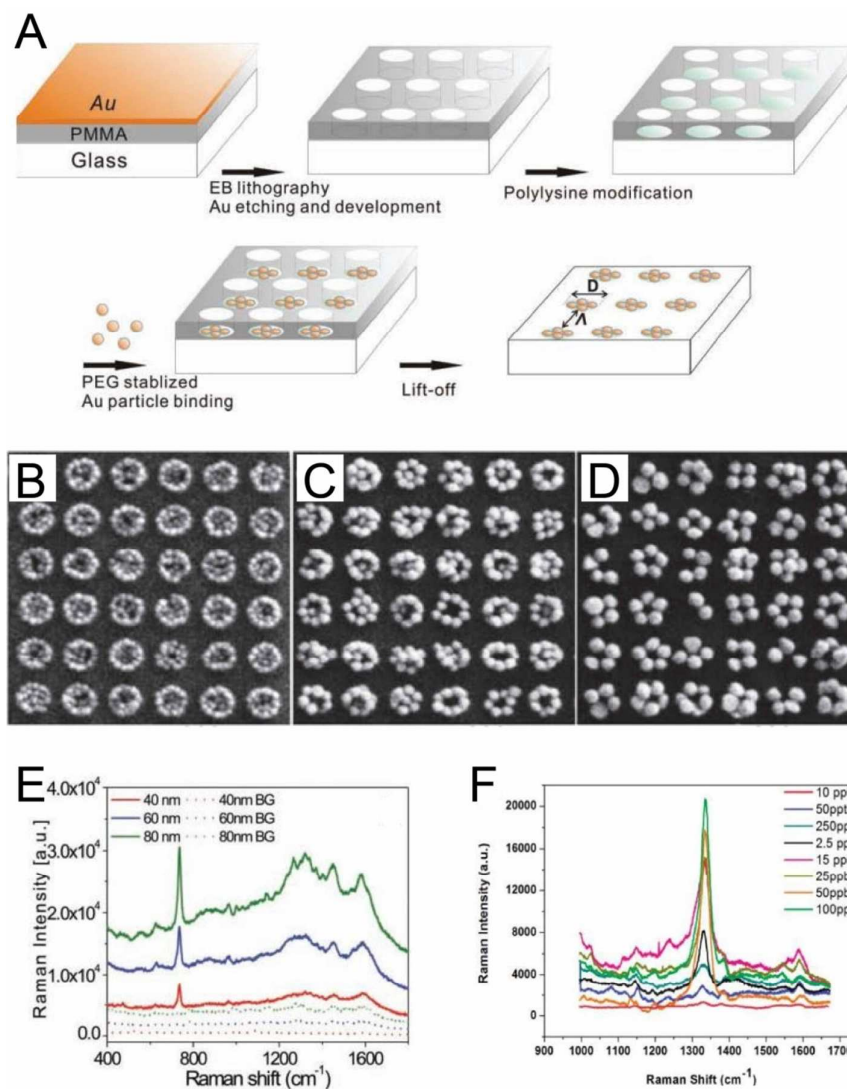


Figure 5. (A) Template assisted NCA assembly on glass substrate. EBL is used to create binding sites in a PMMA mask. These binding sites are functionalized with polylysine. Negatively charged gold nanoparticles are then bound to these cluster binding sites. In a final process step PMMA is removed and the NCA is obtained. (B-D) Typical SEM images of ($D = 200$ nm, $\Lambda = 50$ nm) NCAs. The corresponding diameters are 40, 60, and 80 nm, respectively. (E) SERS spectra (solid) of *B. cereus* on $d = 40, 60, 80$ nm NCAs and corresponding NCA background spectra (dashed). Reproduced with permission from Reference 37. Copyright 2010 WILEY-VCH Verlag GmbH & Co. KGaA, Weinheim. (F) SERS spectra of 2,4-dinitrotoluene measured on NaOH activated NCAs for concentrations between 100 ppb and 10 ppt. Reproduced with permission from Reference 38. Copyright 2011 American Chemical Society.

F. L. Yap et al.³⁹ further improved the NCA generation method, in which an alternative template

of 2D self-assembled ordered polyelectrolyte was used instead of nanowell arrays fabrication by EBL, thereby enabling minimum inter-particle separations of <5 nm, inter-cluster separations of ~10 nm. The demonstrated approach paves the way to significantly low-cost and high throughput production of NCAs.

5

2.2. Q3D structures

2.2.1. Nanohole-disk array

In a recent example, large-area spatially coherent arrays of Q3D plasmonic crystals^{1, 2 14, 40}, which consist of periodically perforated nanoscale holes in a gold film with a gold nanodisk at the bottom of each hole (Fig. 6A), were formed by soft nanoimprint lithography and used for multispectral sensing and imaging of molecular binding events. The arrays were fabricated by embossing a thin UV-curable polyurethane film with a composite hard polydimethylsiloxane (h-PDMS)/PDMS stamp presenting surface relief features in the geometry of a square array of cylindrical posts. The plasmonic devices were found to be of high quality with few pixel defects (< 10) over large areas ($\approx 20 \text{ mm}^2$), as determined by SEM imaging.

The most sensitive peak at ~1023 nm was found to redshift and increased in intensity with progressively more concentrated aqueous solutions of polyethyleneglycol (Fig. 6B); the sensitivity was determined to be $22,000 \Delta\%T \cdot \text{nm}/\text{RIU}$, whilst the peak shift lineary sensitivity was evaluated to be 700-800 nm/RIU. This device was then applied to quantitative analytical bioassay in normal transmission mode, using a well-studied biotin-avidin ligand-receptor conjugate model system (Fig. 6D). Recently investigations showed, based on the finite difference time domain calculations, that it is possible to further optimize the bulk refractive index sensing capabilities of plasmonic crystals³. Changes in the different system parameters (metal film thicknesses, hole diameters and relief depths, etc.) led to an order of magnitude improvement in the figure of merit was predicted. These devices therefore are low-cost platform for performing quantitative biochemical sensing and imaging with extremely high sensitivities in ways that facilitate miniaturization and integration into portable microfluidic lab-on-chip instrumentation.

20
25

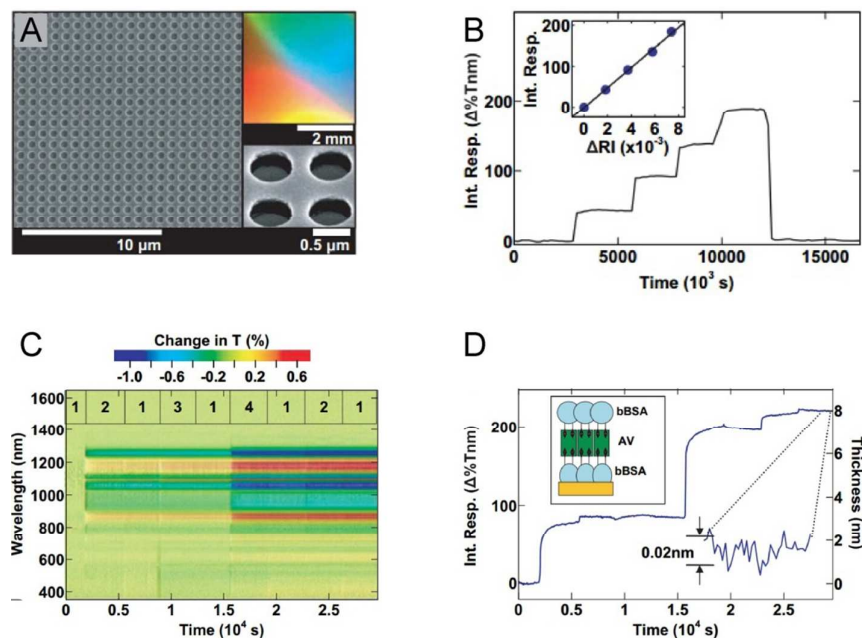


Figure 6. (A) SEM images of a plasmonic nanohole-disk array. Upper inset is an optical image of the structures. Lower inset is a high magnification SEM that shows the upper and lower levels of gold. (B) Integrated multispectral plasmonic response as a function of time. Inset: a linear correlation to the change in refractive index. (C) Color contour plot of the change in transmission as a function of wavelength and time. The overlaid injection sequence corresponds to PBS (1), bBSA (2), BSA (3), and avidin (4). (D) Integrated multispectral plasmonic response and corresponding effective thickness of the biotin-avidin-biotin assay (schematically illustrated in the upper inset). The noise limited refractive index resolution of the crystals corresponds to submonolayer coverages (lower inset). Reproduced with permission from Reference 14. Copyright 2006 National Academy of Sciences.

2.2.2. Gold nanomushroom array

On the consideration of increasing the plasmonic sensor's FOM, which are refractive index sensitivities divided by plasmon resonance linewidths, by simultaneously improving its refractive index sensitivity and reducing its FWHM. Y. Shen et al.¹⁵ constructed a gold nanomushroom array (GNMA) substrate using interference lithography (IL). The structure can be described as a periodic array of mushrooms with gold caps grown on a gold film with a periodic array of holes (Fig 7A). The GNMA array carried out a FOM reaching ~ 108 , which is comparable to the theoretically predicted upper limit for standard propagating surface plasmon resonance (PSPR) sensors. Such a high FOM

arises from, on one hand, the FWHM decrease tremendously at a 30° measuring angle due to the interference between Wood's anomaly (WA) and the LSPRs (Fig. 7B). On the other hand, the apparent refractive index sensitivity of the lifted metal caps was increased because more spatial regions around the gold caps with plasmon-enhanced electric fields will be accessible by the surrounding environment (Fig 7C). This Q3D array structure closely related to the above-mentioned perforated film with nanodisks at the bottom of the nanoholes (*i.e.* nanohole-disk array), and can be thought of as an inverse one to nanohole-disk array. However, the sensing mechanisms of these two types of array structures are very different. The sensing of the reported nanohole-disk structure is based on the interference between WA and the PSPR of the upper perforated gold film¹. In GNMA, the gold caps are on the top of the photoresist pillars, inducing a strong LSPR, and the sensing of GNMA relies on the interference between the LSPRs and WA⁴.

W. B. Li⁴¹ and his co-workers applied the modified GNMA array to rapid detection of alpha-fetoprotein, an important biomarker specific to hepatocellular carcinoma in clinical patient serum, with good anti-interference ability (Fig. 7D). The LOD was determined by alpha-fetoprotein (AFP) standards to be 24 ng/mL (Fig. 7E), which is below the critical concentration (~ 25 ng/mL) in normal plasma. The feasibility for the quantification of AFP in real sample was tested by the serum samples collected from the patients suffered from liver cancer (Fig. 7F), and the results were consistent with the clinical ones reported by electrochemiluminescence immunoassay using a clinical detector (Roche E170), suggesting that the GNMA biosensor qualified in label-free and one-step detection for clinical application. The GNMA array therefore offers an outstanding platform for label-free chemical and biomedical sensing, and high-throughput screening of antibodies and biomarkers in various cases after corresponding functionalization.

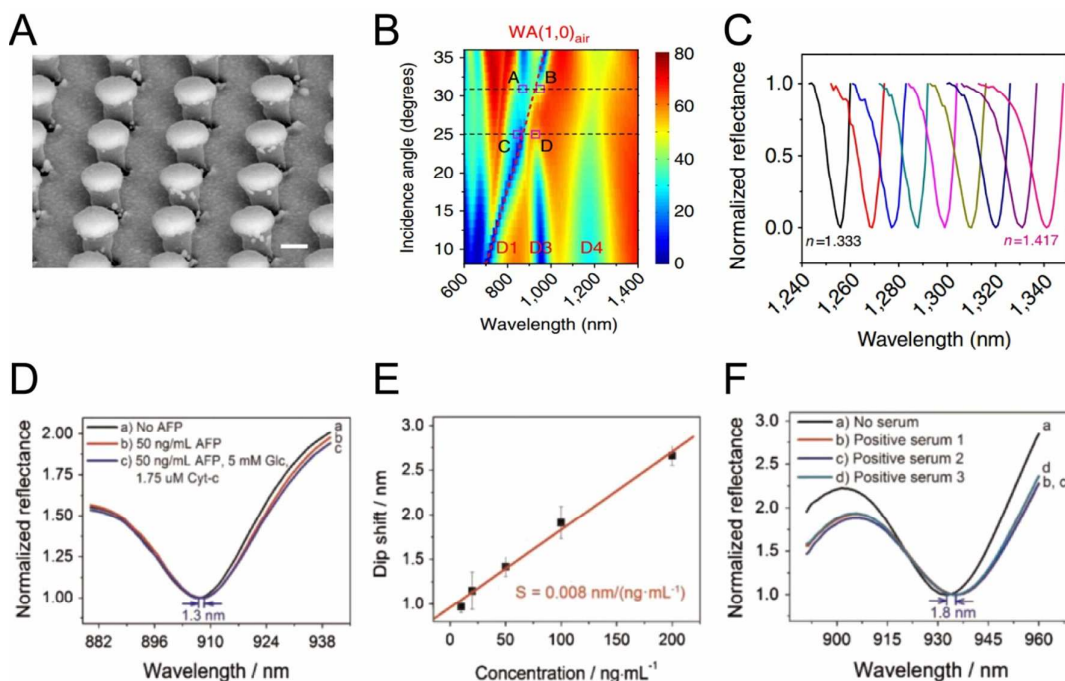


Figure 7. (A) Side-view SEM images of the GNMA. (B) Simulated and reflectance spectra for the incidence angle varied from 8° to 36° at a step of 1° that well agree with the measured ones. The red dashed line in denotes (1, 0) Wood's anomaly. (C) Reflectance spectra of the GMRA immersed in different glycerine-water mixture solutions. Reproduced with permission from Reference 15. Copyright 2006 National Academy of Sciences. 2013 Macmillan Publishers Limited (D) Normalized reflectance spectra measured when the anti-AFP modified GNMA substrate was exposed to phosphate buffer (pH=7.2) (a) without AFP, (b) containing 50 ng/mL AFP solution, and (c) containing a mixture solution of 50 ng/mL AFP, 5 mM Glc and 1.75 μ M Cyt c successively. (E) Relationship between the dip shifts and the AFP concentrations ranging from 10 ng/mL to 200 ng/mL. The line is a linear fit. The error bars in B represent s.d. calculated from three data points measured at each concentration. (F) Normalized reflectance spectra of the GNMA biosensor before (a) and after (b, c and d) it was exposed to a human serum sample three times. Reproduced with permission from Reference 41. Copyright 2015 Elsevier B.V.

2.2.3. Bar-coupled dots-on-pillar cavity array

C. Wang et al.⁴² developed another similar nanostructure called nanobar shaped disk-coupled dots-on-pillar antenna-array (Bar-D2PA), which comprises a dielectric (or semiconductor) bar-shaped pillar array of subwavelength dimensions on a substrate with a metallic bar disk on top of each pillar, a perforated metallic backplane at the pillar foot, and metallic nanodots on the pillar

sidewalls (Fig. 8C). This nanostructure was fabricated through completely by multi-step NIL. Once a nanoimprint mold is made, the Bar-D2PA fabrication is one of the simplest for nanoplasmonic structures. The proposed method allows uniform patterning and flexible design of various nanobar geometries and dimensions. The LSPR peak of this nanostructure array can be effectively tune by just changing the thickness of the deposition metal layer. Although, it has not been applied to biosensing, the device has the potential that is all desirable for optimized IR plasmonic sensors.

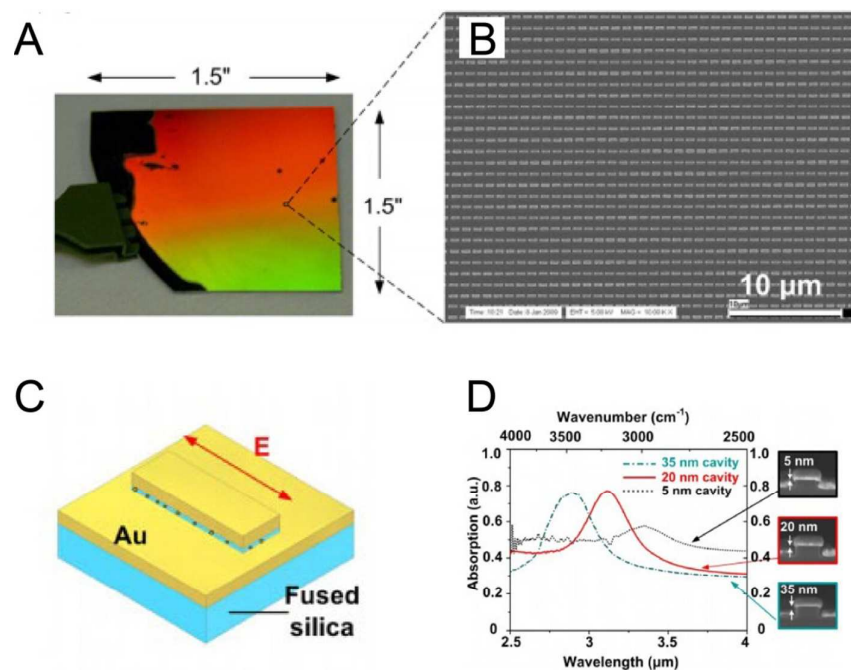


Figure 8. Bar-coupled dots-on-pillar cavity nanostructures and its Fourier Transform Infrared (FTIR) measured IR performance with light polarization along the long-axis. (A) Optical image and (B) large-area top-view SEM image of the array. (C) Schematic of nanostructure and measurement configuration. (D) FTIR-measured absorption spectra of three chips with 5 nm (black dot lines), 20 nm (red solid lines), and 35 nm (dark-cyan dash-dot lines) cavity gaps (the distance between the metal disk and backplane), with the cross-sectional SEM images shown as inserts. The bar-D2PA (700 nm long, 185 nm wide) with nominal gaps of 5, 20 and 35 nm were formed using nominal pillar heights of 55, 70 and 85 nm and an Au film thickness of 50 nm. Reproduced with permission from Reference 42. Copyright 2014 American Chemical Society.

3. Comparisons among the fabrication methods

The development of array-based LSPR sensing elements partially facilitated by various

advanced micro-/nano- fabrication methods, which are conventionally classified into top-down methods and bottom-up methods which involve self-assemble process. Because the bottom-up methods are difficult to form well-designed and uniform nanostructures in large-area, the synthesis of metal plasmonic nanostructures is primarily based on top-down approaches, typically as various lithography techniques employing e-beam, optical, nanosphere, or their derivative methods. The following table summarizes both the advantages and disadvantages of these fabrication methods.

Table 1. Fabrication methods for metal plasmonic nanostructure array

Method	Applications	Requirement	Cost	Resolution	Disadvantages
EBL ⁴³	2D planar nanostructure <i>e.g.</i> Nanohole array	EBL system in clean room	Expensive	< 10 nm	Time-consuming, small area and low throughput
FIB lithography ⁴⁴	2D planar nanostructure <i>e.g.</i> Nanohole array	FIB system in clean room	Expensive	10 nm	Time-consuming, small area
Optical lithography ⁴³	2D: nanohole array, Nanohole-disk array, Q3D: GNMA	Optical lithography system, clean room	High-cost	10-20 nm	Multiple steps; incompatible with organic solvent
NSL ^{31, 45}	2D shape-limited metal island	Normal lab conditions	Low-cost	~50 nm	Shape-limited; more pattern defects
NIL ⁴⁶ and soft lithography ⁴⁷	2D Nanohole array, nanohole-disk array, Q3D GNMA*	Normal lab conditions	Low-cost	20-30 nm	More pattern defects
Colloidal lithography ¹³	2D Metal island	Normal lab conditions	Low-cost	NG	Non-uniform
Electrochemi- cal etching ⁴⁸	2D and Q3D: Al nanoconcave array, nanocone array*	Normal lab conditions	Low-cost	NG	Weak controllability
Self-assembly ³⁹	2D, <i>e.g.</i> NCA	Normal lab conditions	Low-cost	< 5nm	More pattern defects, weak controllability

Note: (1) NG means not given in literature. (2) * represents the unpublished data from our group.

In a word, EBL and FIB lithography are mature techniques that allow controlling precisely size, shape and interparticle distance of the surface bound metallic nanostructures; however, they are not suitable for large-area and high through-put generation. NIL and soft lithography considered to be the next generation lithographic techniques are higher through-put and larger-area; however, the precision and anti-deformation need to be further improved. So far, optical lithography, though sustains multiple-steps procedure and possible slight changes among bathes, is the irreplaceable method for 2D and 3D nanostructure generation both in industry and in laboratory. To overcome these limitations of different micro/nano fabrication techniques, researches tend to combine top-down and bottom-up methods, such as generation of NCAs using template-assisted self-assembly strategy³⁹.

4. Perspectives

4.1. Improve the sensor's refractive index sensitivity and FOM

Taken as the observable advantages compared with some other conventional methods such as electrochemical sensing⁴⁹, enzyme-linked immune sorbent assay⁵⁰, and fluorescent immunoassay⁵¹, LSPR sensing enjoys a reputation of both label-free and one-step that are crucial for rapid detection and real-time biosensing. It is inherently more timesaving and more economic than other endpoint analyses, because it requires only single antibody and provides direct detection without extensive detection protocols. Unfortunately, the low refractive index sensitivity of LSPR nanostructures hinders its wide applications. Hence, much more efforts have been made to improve the refractive index sensitivity.

In general, changing the size and shape⁵², and the pattern arrange⁵³ are effective methods to tune the plasmonic mode and the refractive index sensitivity. The results obtain by H. J. Chen⁵⁴ showed that, sharp nanoparticle features give rise to hot-spots in the electromagnetic fields that increase the sensitivity to local refractive index and amplify surface-enhanced Raman spectroscopy signals as well. In addition, by lifting up the nanoparticles⁵⁵ or partially etching away the adjacent substrate⁵⁶, the refractive index sensitivity of the substrate will be increased, because there are much spatial regions with plasmon-enhanced electric fields that will be accessible by the target molecules. There have also been some interests in the LSPR sensing capabilities of nanostructures exhibiting Fano resonances in their extinction spectra^{57, 58}. Fano resonances arise in asymmetrical nanostructures

(such as nonconcentric core shell particles) when a typical, “bright” plasmon mode which couples to light, interferes with a “dark” plasmon mode which does not couple to light. The result is a sharp dip in the extinction, which is theoretically predicted to have extremely high refractive index sensitivity and FOM.

5 On the other one hand, the refractive index sensitivity can also be influenced by the material used as the substrate⁵⁹ and the surface organic coating⁶⁰ which is used to create specificity for biosensing. The supporting substrates (typically glass) possess a RI that is much higher than those corresponding to the buffer solutions normally used in bioassays. As a consequence, the symmetry of the electromagnetic around the nanostructures is broken, shifting a much larger part of this electric and magnetic field toward the metal/glass interface, significantly lowering the overall sensitivity of the nanoplasmonic structures⁶¹. Therefore the use of low RI materials as supporting substrates presents itself as a very straightforward method to overcome this problem. Also, by tuning the molecules used for surface modification, the refractive index sensitivity can also be improved. According to the theoretical simulation, the maximum local field factor of LSPR varied with the thickness and the dielectric constant of the coated layers⁵⁹. For an experimental example, the sensitivity of the GNMA after it was surfacially modified was much lower than the one when it was bare⁴¹. One interesting strategy takes advantage of thiol place exchange processes. Beeram et al.⁶² followed this procedure by firstly covering the surface with a non-reactive thiol. Then, these non-reactive thiols were subsequently exchanged by another thiol-modified compound, occurring preferentially at vertex sites of the nanostructures (which turned out to be approximately 2–3 times more sensitive than terrace sites). Another interesting strategy utilizes the advantage of modifying only the desired locations with reactive molecules, while blocking the other surface area. W. B. Li et al.⁴¹ complied with this route by modifying only the caps of the GNMA, which served as the maximum electron intensity distribution area. In this case, the MUA were firstly spin-coated on a flat PDMS film; after drying, the PDMS stamp was brought contact to the GNMA surface, resulting in MUA self-assemble only on the caps. The unbind area was then blocked by the non-reactive molecules. By only exposing the highly sensitive inner walls of the nanoholes to the surrounding dielectric, L. Feuz and his co-authors⁶³ assured the binding of molecules to the most sensitive regions of the transducer surface as well.

30

4.2. Use normal transmission LSPR sensing mode

As mentioned in the previous section, T-LSPR is eye-catching owing to its simplicity, low-cost, and ease-of-use configuration^{64,65}. On one hand, T-LSPR sensing offers greater prospective for both the highly-parallel integrated device and the simple, low-cost optical setup due to its transmission configuration in comparison with reflection LSPR sensing. On the other hand, T-LSPR performed in normal transmission mode are more attractive; because it does not need the incident angle to be readjusted when the light source passes through the materials, solvents or analytes with different RI, whilst the RI of solutions are slightly changed by the analytes all through the concentration-dependent measurements. The changes caused by different concentrations of analytes can not be quantified and fed forward to optimize the oblique incident angle of the LSPR sensors, which introduces the systematic errors; but, such errors could be eliminated in normal transmission mode. To perform a T-LSPR, the sensing substrate thereafter needs fine optical transmission, the transparent materials are the best choice; besides, the nanostructure must be designed thin enough or allow perforation intervals on the metal arrays. According to the analysis above, the ordered nanohole array and the particle array created using NSL, as well as some other quasi-three-dimensional nanostructures, therefore the good choices for normal T-LSPR sensing.

4.3. Integrate the plasmonic sensor on a chip

It is no doubt that, LSPR biosensing performing on microfluidic chip when the sensing array substrate are integrated on is the irreversible trends, though the majority of recent publications keep being limited to a proof-of-concept based on a routine biomolecule immobilization and subsequent target detection, partially due to the reason listed above as the insufficient sensitivity and the configuration designation. The on-chip LSPR sensing also face the challenges of reproducibility, sensitivity, specificity and viability to detect targets in complex samples. Perhaps the one most close to on-chip practice is the ordered nanohole array. Seeing that there has been excellent reviews on nanohole array based sensing^{66,67}, we will not discuss it here.

The other nanostructures, such as nanohole-disk, islands, and GNMA are also capable of on-chip biosensing. As a simple demonstration, the nanohole-disk array was integrated on a five-channel chip for the nonspecifically adsorbed fibrinogen (Fig. 9A). The chip can be used in T-LSPR mode, as showed in the below, which involves a white light source, monochromater,

imaging optics, and a CCD array detector, suggesting a promising platform for performing parallel diagnostic bioassays¹⁴. The nanodisk array prepared by colloid lithography is a well-studied model set of on-chip sensing¹³. As illustrated in an optical image (Fig. 9B), the setup consists of a compact white light source, a sensing chip that is an assembly of glass-supported Au nanostructures enclosed in a simple stainless steel fluidics device with the analyte solution kept at static conditions once injected, and a miniature spectral analyzer coupled to a personal computer. The light spot for excitation is about $\sim 0.13 \text{ cm}^2$. This configuration is capable of label-free and real-time biosensing of multiple analytes, and the integration density could be thereafter tuned according to the area of the light spot.

10

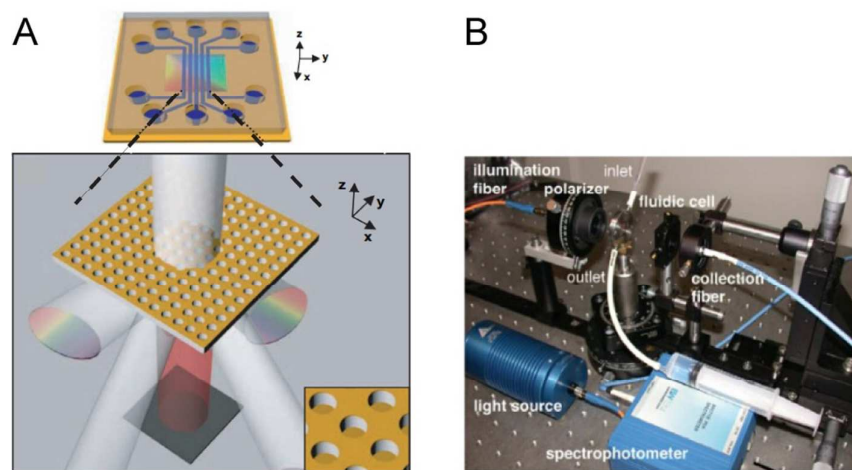


Figure 9. (A) A multichannel PDMS microfluidic network used to pattern the surface of a plasmonic substrate; the image below schematically illustrates the normal transmission mode geometry used to probe this device. Reproduced with permission from Reference 14. Copyright 2006 National Academy of Sciences. (B) Experimental setup for on-chip sensing using the nanodisk array generated through colloid lithography. Reproduced with permission from Reference 13. Copyright 2009 IOP Publishing Ltd.

4.4. Explore aluminum plasmonics for biosensing

As an overview in recent one decade, aluminum plasmonic increasingly attracted researchers on its unparalleled properties of low-cost, high natural abundance, and ease of processing by a wide variety of methods including CMOS, and the UV to blue plasmons induced by its inherent dielectric properties. There has been several groups pay their attentions on aluminum plasmonic biosensing.

Except for the nanohole array reviewed in section 2, aluminum nanoconcaves array fabricated by electrochemical etching were also successfully applied to biosensing by M. Norek and his co-workers⁴⁸. As shown in Fig. 10, the sensitivity of this nanoconcave structure can be tune by changing the voltage adopted for electrochemical etching. The sensitivities of two types of nanoconcaves generated at 120 V and 195 V were determined to be 190 and 420 nm/RIU, respectively.

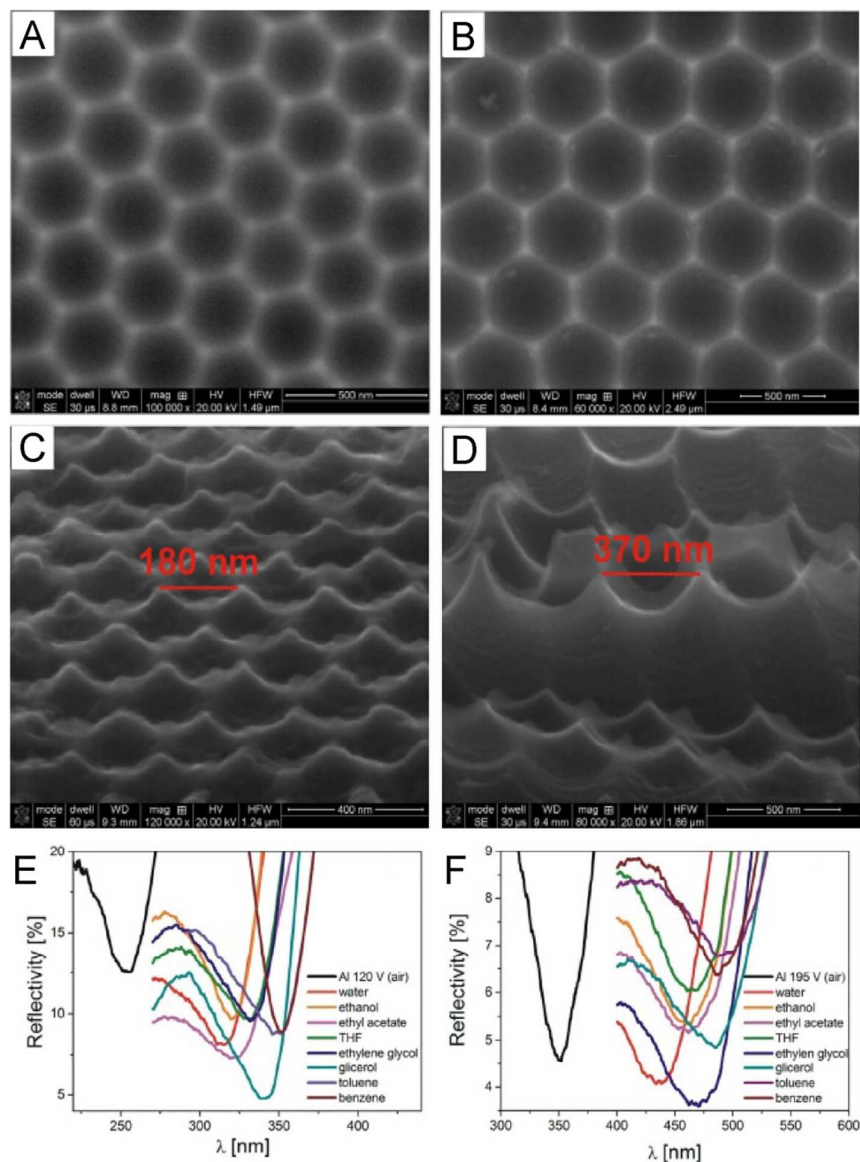


Figure 10. Top-view SEM images of Al concaves fabricated at 120 V (A) and at 195 V (B). (C) and (D) demonstrate an angle view of the Al concaves fabricated at 120 V and 195 V, respectively. (E) and (F) are the reflectance spectra of the Al concaves fabricated at 120 V and 195 V when exposed to different organic solvents. Reproduced with permission from Reference 48. Copyright 2014 Elsevier

B.V.

Despite its great potential and the effort made recently, biosensing using aluminum plasmonics are still in its infancy and facing a variety of challenges from two view-points of fabrication technique and improving the sensitivity. Aluminum is significantly more difficult to be synthesized in the few nanometer size regimes⁶⁸, and the outer metallic layer quickly oxidizes upon exposure to atmosphere⁶⁹ in comparison with its Au and Ag noble metal counterparts. Whilst Al LSPRs much more sensitive than those of most other materials to the nanoparticle geometrical characteristics⁷⁰. These strong size and shape dependent lead aluminum plasmonics to the inevitable disadvantages, such as useless spectra, in the absence of narrow particle size distributions, and sharp LSPRs quickly turning into broad. Also, the present aluminum plasmonics sustained low refractive index sensitivities^{26-28, 48}. Al nanostructure with high RI sensitivities from UV to infrared wave regions for high-performance biosensing is urgent for application as well. Maybe the fast route for overcome these difficulties is to imitate the lessons we learned from gold and silver plasmonic to establish well-designed 2D or even Q3D array nanostructures.

5. Conclusions

In conclusion, we reviewed the latest well-designed metallic nanostructures for plasmonic biosensing. These 2D and Q3D array based nanostructures show great potential to be mass integrated on microfluidic chips, and enable low-cost, convenient, and easy-of-use platforms for high through-put biosensing. Recent progresses in micro- and nano- fabrication techniques have also boost the new plasmonic structure generation, which meet the commercial needs of low-cost and facile. The future trends of the well-designed plasmonic lie in: (1) improving the refractive index sensitivity that high enough to carry out direct and label-free biosensing; (2) simplifying the optical configuration, such as by adopting the T-LSPR mode; (3) integrating these sensing substrate on microfluidic chips for low-cost, low reagent-consumption and high through-put biosensing; and (4) exploiting the potentialities of biosensing using aluminum plasmonics. It is sincerely hoped that this review will inspire researchers to make their own contributions to this exciting and highly relevant field.

30

Acknowledgments

This work was supported by the National Natural Science Foundation of China (21405183), the project for Science & Technology New Star of Zhujiang in Guangzhou City (2013J2200048), the Science and Technology Innovation Plan (JCYJ20120831160213584), and the project for General Administration of Quality Supervision, Inspection, and Quarantine of the People's Republic of China (2014IK101).

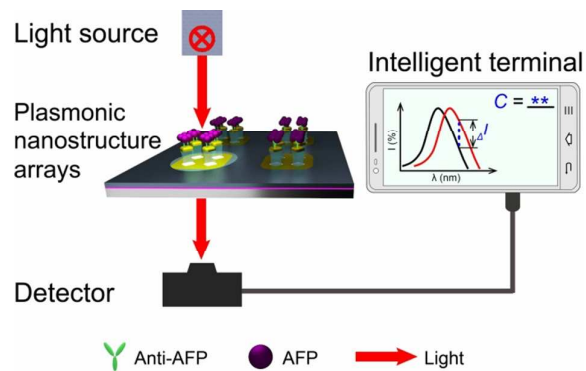
References:

1. S. Kim, J. Jin, Y. Kim, I. Park, Y. Kim and S. Kim, *Nature*, 2008, **453**, 757-760.
2. D. Lim, K. Jeon, H. M. Kim, J. Nam and Y. D. Suh, *Nat. Mater.*, 2009, **9**, 60-67.
3. A. V. Kabashin, P. Evans, S. Pastkovsky, W. Hendren, G. A. Wurtz, R. Atkinson, R. Pollard, V. A. Podolskiy and A. V. Zayats, *Nat. Mater.*, 2009, **8**, 867-871.
4. K. M. Mayer and J. H. Hafner, *Chem. Rev.*, 2011, **111**, 3828-3857.
5. X. Lu, M. Rycenga, S. E. Skrabalak, B. Wiley and Y. Xia, *Annu. Rev. Phys. Chem.*, 2009, **60**, 167-192.
6. J. L. Wilbur, A. Kumar, H. A. Biebuyck, E. Kim and G. M. Whitesides, *Nanotechnology*, 1996, **7**, 452.
7. D. Gérard and S. K. Gray, *Journal of Physics D: Applied Physics*, 2015, **48**, 184001.
8. G. H. Chan, J. Zhao, E. M. Hicks, G. C. Schatz and R. P. Van Duyne, *Nano Lett.*, 2007, **7**, 1947-1952.
9. A. Tittl, P. Mai, R. Taubert, D. Dregely, N. Liu and H. Giessen, *Nano Lett.*, 2011, **11**, 4366-4369.
10. J. T. Kim and S. Y. Choi, *Opt. Express*, 2011, **19**, 24557-24562.
11. A. Lesuffleur, H. Im, N. C. Lindquist, K. S. Lim and S. Oh, *Opt. Express*, 2008, **16**, 219-224.
12. Y. H. Lee, C. K. Lee, B. Tan, J. M. Rui Tan, I. Y. Phang and X. Y. Ling, *Nanoscale*, 2013, **5**, 6404.
13. S. Chen, M. Svedendahl, M. Kall, L. Gunnarsson and A. Dmitriev, *Nanotechnology*, 2009, **20**, 434015.
14. M. E. Stewart, N. H. Mack, V. Malyarchuk, J. A. Soares, T. W. Lee, S. K. Gray, R. G. Nuzzo and J. A. Rogers, *Proc. Natl. Acad. Sci. USA*, 2006, **103**, 17143-17148.
15. Y. Shen, J. Zhou, T. Liu, Y. Tao, R. Jiang, M. Liu, G. Xiao, J. Zhu, Z. Zhou, X. Wang, C. Jin and J. Wang, *Nat. Commun.*, 2013, **4**, 2381-2389.
16. A. A. Tseng, *Small*, 2005, **1**, 594-608.
17. M. Rothschild, T. M. Bloomstein, N. Efremow, T. H. Fedynyshyn, M. Fritze, I. Pottebaum and M. Switkes, *MRS Bull.*, 2005, **30**, 942-946.

18. M. C. Daniel and D. Astruc, *Chem. Rev.*, 2004, **104**, 293-346.
19. A. G. Brolo, R. Gordon, B. Leathem and K. L. Kavanagh, *Langmuir*, 2004, **20**, 4813-4815.
20. C. Huang, P. Chiu, Y. Wang and C. Yang, *J. Colloid. Interf. Sci.*, 2006, **303**, 430-436.
21. T. W. Ebbesen, H. J. Lezec, H. F. Ghaemi, T. Thio and P. A. Wolff, *Nature*, 1998, **391**, 1947-1952.
- 5 22. H. Gao, J. Henzie and T. W. Odom, *Nano Lett.*, 2006, **6**, 2104-2108.
23. J. Masson, M. Murray-Méhot and L. S. Live, *Analyst*, 2010, **135**, 1483.
24. A. De Leebeeck, L. K. S. Kumar, V. de Lange, D. Sinton, R. Gordon and A. G. Brolo, *Anal. Chem.*, 2007, **79**, 4094-4100.
25. F. Eftekhari, C. Escobedo, J. Ferreira, X. Duan, E. M. Girotto, A. G. Brolo, R. Gordon and D. Sinton, *Anal. Chem.*, 2009, **81**, 4308-4311.
- 10 26. J. L. Skinner, L. L. Hunter, A. A. Talin, J. Provine and D. A. Horsley, *IEEE T. Nanotechnol.*, 2008, **7**, 527-531.
27. V. Canalejas-Tejero, S. Herranz, A. Bellingham, M. C. Moreno-Bondi and C. A. Barrios, *ACS Appl. Mater. Inter.*, 2014, **6**, 1005-1010.
- 15 28. C. A. Barrios, V. Canalejas-Tejero, S. Herranz, M. C. Moreno-Bondi, M. Avella-Oliver, R. Puchades and A. Maquieira, *Plasmonics*, 2014, **9**, 645-649.
29. B. Zhang, R. B. Kumar, H. Dai and B. J. Feldman, *Nat. Med.*, 2014, **20**, 948-953.
30. J. Chen, J. Qui, S. Fan, S. Kuo, F. Ko, C. Chu and F. Chang, *J. Colloid. Interf. Sci.*, 2012, **367**, 40-48.
31. R. P. V. D. John C. Hulteen, *J. Vac. Sci. Technol. A*, 1995, **3**, 1553-1558.
- 20 32. C. L. Haynes and R. P. Van Duyne, *J. Phys. Chem. B*, 2001, **105**, 5599-5611.
33. J. Dickmann, *J. Electrochem. Soc.*, 1991, **138**, 491.
34. M. D. Malinsky, K. L. Kelly, G. C. Schatz and R. P. Van Duyne, *J. Am. Chem. Soc.*, 2001, **123**, 1471-1482.
35. T. Jensen, L. Kelly, A. Lazarides and G. C. Schatz, *J. Clust. Sci.*, 1999, **10**, 295-317.
- 25 36. B. Yan, A. Thubagere, W. R. Premasiri, L. D. Ziegler, L. Dal Negro and B. M. Reinhard, *ACS Nano*, 2009, **3**, 1190-1202.
37. L. Yang, B. Yan, W. R. Premasiri, L. D. Ziegler, L. D. Negro and B. M. Reinhard, *Adv. Funct. Mater.*, 2010, **20**, 2619-2628.
38. J. Wang, L. Yang, S. Boriskina, B. Yan and B. M. Reinhard, *Anal. Chem.*, 2011, **83**, 2243-2249.
- 30 39. F. L. Yap, P. Thoniyot, S. Krishnan and S. Krishnamoorthy, *ACS Nano*, 2012, **6**, 2056-2070.

40. J. Yao, A. Le, S. K. Gray, J. S. Moore, J. A. Rogers and R. G. Nuzzo, *Adv. Mater.*, 2010, **22**, 1102-1110.
41. W. Li, X. Jiang, J. Xue, Z. Zhou and J. Zhou, *Biosens. Bioelectron.*, 2015, **68**, 468-474.
42. C. Wang, Q. Zhang, Y. Song and S. Y. Chou, *ACS Nano*, 2014, **8**, 2618-2624.
43. S. Okazaki, *Microelectron. Eng.*, 2015, **133**, 23-35.
- 5 44. K. Gamo, *Nuclear Instruments and Methods in Physics Research Section B: Beam Interactions with Materials and Atoms*, 1992, **65**, 40-49.
45. W. Li, L. Xu, W. Zhao, P. Sun, X. Huang and K. Chen, *Appl. Surf. Sci.*, 2007, **253**, 9035-9038.
46. M. Li, J. Wang, L. Zhuang and S. Y. Chou, *Appl. Phys. Lett.*, 2000, **76**, 673.
47. X. Zhao, Y. Xia and G. M. Whitesides, *J. Mater. Chem.*, 1997, **7**, 1069-1074.
- 10 48. M. Norek, M. Włodarski and P. Matysik, *Curr. Appl. Phys.*, 2014, **14**, 1514-1520.
49. H. Su, R. Yuan, Y. Chai, L. Mao and Y. Zhuo, *Biosens. Bioelectron.*, 2011, **26**, 4601-4604.
50. H. Ju, G. Yan, F. Chen and H. Chen, *Electroanal.*, 1999, **11**, 124-128.
51. T. K. Christopoulos and E. P. Diamandis, *Anal. Chem.*, 1992, **64**, 342-346.
52. K. Lee and M. A. El-Sayed, *J. Phys. Chem. B*, 2006, **110**, 19220-19225.
- 15 53. T. Atay, J. Song and A. V. Nurmikko, *Nano Lett.*, 2004, **4**, 1627-1631.
54. H. Chen, X. Kou, Z. Yang, W. Ni and J. Wang, *Langmuir*, 2008, **24**, 5233-5237.
55. A. Dmitriev, C. Hägglund, S. Chen, H. Fredriksson, T. Pakizeh, M. Käll and D. S. Sutherland, *Nano Lett.*, 2008, **8**, 3893-3898.
56. N. A. Hatab, C. Hsueh, A. L. Gaddis, S. T. Retterer, J. Li, G. Eres, Z. Zhang and B. Gu, *Nano Lett.*, 2010,
20 **10**, 4952-4955.
57. I. M. Pryce, Y. A. Kelaita, K. Aydin and H. A. Atwater, *ACS Nano*, 2011, **5**, 8167-8174.
58. N. Verellen, P. Van Dorpe, C. Huang, K. Lodewijks, G. A. E. Vandenbosch, L. Lagae and V. V. Moshchalkov, *Nano Lett.*, 2011, **11**, 391-397.
59. M. C. Estevez, M. A. Otte, B. Sepulveda and L. M. Lechuga, *Anal. Chim. Acta*, 2014, **806**, 55-73.
- 25 60. C. Min, W. Meng and G. Ning, *Chinese Phys. Lett.*, 2009, **26**, 45201.
61. M. M. Miller and A. A. Lazarides, *J. Phys. Chem. B*, 2005, **109**, 21556-21565.
62. S. R. Beeram and F. P. Zamborini, *J. Am. Chem. Soc.*, 2009, **131**, 11689-11691.
63. L. Feuz, P. Jönsson, M. P. Jonsson and F. Höök, *ACS Nano*, 2010, **4**, 2167-2177.
64. E. Hutter and M. Pileni, *J. Phys. Chem. B*, 2003, **107**, 6497-6499.
- 30 65. Y. Shon, H. Y. Choi, M. S. Guerrero and C. Kwon, *Plasmonics*, 2009, **4**, 95-105.

66. R. Gordon, D. Sinton, K. L. Kavanagh and A. G. Brolo, *Acc. Chem. Res.*, 2008, **41**, 1049-1057.
67. C. Escobedo, *Lab Chip*, 2013, **13**, 2445.
68. M. J. Meziani, C. E. Bunker, F. Lu, H. Li, W. Wang, E. A. Gulians, R. A. Quinn and Y. Sun, *ACS Appl. Mater. Inter.*, 2009, **1**, 703-709.
- 5 69. E. Stratakis, M. Barberoglou, C. Fotakis, G. Viau, C. Garcia and G. A. Shafeev, *Opt. Express*, 2009, **17**, 12650-12659.
70. F. Bisio, R. Proietti Zaccaria, R. Moroni, G. Maidecchi, A. Alabastri, G. Gonella, A. Giglia, L. Andolfi, S. Nannarone, L. Mattera and M. Canepa, *ACS Nano*, 2014, **8**, 9239-9247.



Well-designed metal nanostructured array holds great advantages for on-chip label-free plasmonic biosensing, meeting the need for portable and rapid diagnosis.